# Effect of spin-orbit interaction on circular current: Pure spin current phenomena within a ring conductor

## Moumita Patra<sup>1</sup>

<sup>1</sup>Department of Physics, Indian Institute of Science Education and Research, Pune 411008, India

A net circulating current may appear within a quantum ring under finite bias. We study the characteristic features of the circular current in the presence of Rashba spin-orbit interaction (RSOI). Both charge and spin currents appear within the ring. Whereas when the ring is symmetrically connected to the external leads, we can get a pure charge current at non-zero Fermi-energy. On the other hand, for asymmetric ring-to-leads configuration, at zero Fermi-energy, the spin current vanishes but a pure charge current flows within the ring. Tuning RSOI, we demonstrate a way to control the pure spin current externally. This new perspective of the generation of the pure spin circular current can open a new basis for the highly efficient, low energy cost spintronic devices.

# I. INTRODUCTION

In the context of quantum transport, we generally focus on the overall conduction properties of a junction. But when the bridging conductor contains a loop structure, there is a possibility to induce a circular current within the loop. Circular current may behave very differently and may have a very large magnitude compared to the overall drain current. The circular current may appear within a quantum loop under several circumstances. In the early 80's Büttiker et al. first proposed theoretically that a small conducting ring carries a net circulating charge current, commonly known as persistent current in the presence of the magnetic field. Followed by this, there were lots of theoretical as well as experimental propositions<sup>2-7</sup> in this direction. Using phase-locked infra-red laser pulses circular current has been generated in an isolated quantum ring<sup>8</sup>. Several other theoretical works have indicated the possibility to excite such loop currents by using external radiation<sup>9</sup>, shaped photon pulses<sup>10,11</sup>, circularly polarized light<sup>12</sup>, twisted light<sup>13</sup>, etc. Circular current can be also induced in quantum rings driven by an external voltage<sup>14–19</sup>. For example, S. Nakanishi and M. Tsukada<sup>20</sup> have predicted the existence of a quantum internal current through the C<sub>6</sub>0 molecular bridge. Large loop currents circulating around the zigzag and chiral carbon nanotubes have been observed by N. Tsuji et.al.<sup>21</sup>. The circular currents due to different driving forces are closely related in nature.

Though the idea of bias induced circular current is so far limited to theoretical computations, but it involves various important factors in the context of quantum transport. Such as, it gives the measurement of current through the individual section of a complicated quantum loop system consists of multiple pathways. Depending on the voltage bias, circular current may rise to a very high value compared to the overall drain current ( $\sim 10^3$  times larger) at the outgoing leads. This giant circular current induces a large magnetic field (in some cases it may even reach to few millitesla or even Tesla) at the center of the ring, which is very important in the context of local spin regulation and several other electronic and spintronic applications like storage of data, logic functions, spin switching, spin-selective electron transmission, spinbased quantum computations,  $etc^{22-26}$ .

In a recent work<sup>19</sup>, the idea of spin circular currents has

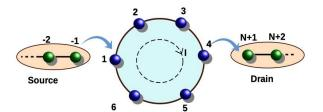


FIG. 1: (Color online). Schematic-representation of the Tight-Binding quantum ring, attached with two semi-infinite electrodes.

been addressed, where the spin components have been defined by the conservation law between the bond current and transport current in a one-dimensional quantum chain. With this formulation, here we make an in-depth analysis on the effect of the Rashba spin-orbit interaction (RSOI) on the bias induced-circular current. RSOI is originated due to the structure inversion asymmetry caused by the inversion asymmetry of the confining potential<sup>27</sup>. It<sup>28,29</sup> is an electrically tunable spin-orbit interaction<sup>30</sup>.

Generation of pure spin current is the ultimate requirement for the spintronic devices, which have evolved from exploiting spin-polarized current to pure spin current. It helps in gaining speed, miniaturization, and high energy efficiency $^{31,32}$  as in this case only electron-spin carries the information. The energy dissipation due to Joule heating, which is the main source of the power dissipation in conventional electronic devices, can be completely suppressed here. It also allows to have spin-orbit torque, different from the spin-transfer torque, which can switch ferromagnetic free layers to design high-density memory devices<sup>33</sup>. The spin Hall effect<sup>34</sup>, spin pumping<sup>35</sup>, ferromagnetic and anti-ferromagnetic metals and insulators are the few ways to generate pure spin current. Here we propose a new idea to generate pure spin current using RSOI. The model is composed of a quantum wire attached to two external baths as shown in Fig. 1. The entire system is non-magnetic and metallic. RSOI is considered at the bridging ring. Under the symmetric ring-to-lead configuration (when the length of the upper arm of the ring is equal to the length of the lower one) the system has two-fold degeneracy along with the spindegeneracy. In this situation, the currents at the two arms of the ring are equal and opposite to each other, resulting in a zero charge circular current. In the presence of RSOI, when unpolarized electrons are injected, it becomes polarized within the ring in such a way that the charge current becomes zero. Hence a pure spin current is generated within the ring. Here the up spin moves to the opposite direction in the down spin. Though the outgoing drain current always remains unpolarized for symmetric as well as asymmetric configurations (when the arm lengths of the ring are unequal). The spin current density is anti-symmetric around incident energy E equals to 0. Therefore we need to set a non-zero Fermi energy to get pure spin circular current.

The conversion of the pure spin current to the pure charge current is also possible here. In an asymmetric junction, if we set the Fermi-energy at zero, the spin current vanishes, resulting in a pure charge current. We find that the spin current is very robust against the connection positions of the electrodes to the ring, unlike the charge current. To make the spin-based quantum computers and other spintronic devices, proper spin regulation is highly important. Tuning the strength of RSOI, we propose a suitable way to control the pure spin current externally. Based on the tight-binding (TB) framework we compute the circular current using wave-guide formalism<sup>18,19,36–38</sup>. With this approach, one can find current carried by each section of the ring. Circular current may decrease with voltage (showing negative differential resistance, NMR) contrary to the overall drain current which increases with voltage.

The arrangement of the remaining part is as follows. In sec. II we thoroughly discussed the methodology to calculate the current in the presence of SOI. In sec. III, we illustrate all the essential results, and finally, we summarize our findings in sec. IV.

## II. THE MODEL AND THEORY

## A. Hamiltonians

The Hamiltonian H for the entire system (shown in Fig. 1) can be written as the sum of the Hamiltonians for the ring  $H_R$ , the electrodes (namely, source S and drain D)  $H_{(S/D)}$ , and the tunneling between the ring and electrodes  $H_T$ . Therefore,

$$H = H_R + H_{(S/D)} + H_T.$$
 (1)

 $H_R$  represents the Hamiltonian for a one-dimensional quantum ring with spin-orbit interaction (SOI), having the TB<sup>39,40</sup> form:

$$H_{R} = \sum_{n} c_{n}^{\dagger} \boldsymbol{\epsilon}_{n} \boldsymbol{c}_{n} + \sum_{n} \left( c_{n+1}^{\dagger} t \boldsymbol{c}_{n} + c_{n}^{\dagger} t \boldsymbol{c}_{n+1} \right)$$
$$- \sum_{n} \left( c_{n+1}^{\dagger} \left( \imath \boldsymbol{\sigma}_{x} \right) \boldsymbol{\alpha} \cos \phi_{n,n+1} \boldsymbol{c}_{n} + h.c. \right)$$
$$- \sum_{n} \left( c_{n+1}^{\dagger} \left( \imath \boldsymbol{\sigma}_{y} \right) \boldsymbol{\alpha} \sin \phi_{n,n+1} \boldsymbol{c}_{n} + h.c. \right). (2)$$

n is the site-index runs from 1 to N, where N is the number of sites in the ring. The other factors are:

$$m{\epsilon}_n = \left( egin{array}{cc} \epsilon_{n,\uparrow} & 0 \\ 0 & \epsilon_{n,\downarrow} \end{array} 
ight), \, m{t} = \left( egin{array}{cc} t & 0 \\ 0 & t \end{array} 
ight), \\ m{c}_n = \left( egin{array}{cc} c_{n,\uparrow} \\ c_{n,\downarrow} \end{array} 
ight), \, m{lpha} = \left( egin{array}{cc} lpha & 0 \\ 0 & lpha \end{array} 
ight).$$

 $\epsilon_{n,\uparrow(\downarrow)}$  represents the on-site potential of an up (down) spin electron. We consider  $\epsilon_{n,\uparrow}=\epsilon_{n,\downarrow}=\epsilon_n$  for the sake of simplicity.  $\alpha$  is the Rashba spin-orbit coupling strength.  $\phi_{n,n+1}=\left(\phi_n+\phi_{n+1}\right)/2$ , with  $\phi_n=2\pi(n-1)/N$ .  $\sigma_i$ 's  $(i=x,\,y,\,z)$  are the Pauli spin matrices in  $\sigma_z$  diagonal representation.  $i=\sqrt{-1}$ .

The Hamiltonian  $H_{(S/D)}$ , representing the electrodes, characterized by the onsite potential  $\epsilon_0$  and the nearest neighbor hopping integral  $t_0$  has the form:

$$H_{S/D} = \sum_{n \leq -1} \boldsymbol{a}_{n}^{\dagger} \boldsymbol{\epsilon}_{0} \boldsymbol{a}_{n} + \sum_{n \leq -1} \left( \boldsymbol{a}_{n+1}^{\dagger} \boldsymbol{t}_{0} \boldsymbol{a}_{n} + \boldsymbol{a}_{n}^{\dagger} \boldsymbol{t}_{0} \boldsymbol{a}_{n+1} \right)$$

$$+ \sum_{n \geq N+1} \boldsymbol{b}_{n}^{\dagger} \boldsymbol{\epsilon}_{0} \boldsymbol{b}_{n} + \sum_{n \geq N+1} \left( \boldsymbol{b}_{n+1}^{\dagger} \boldsymbol{t}_{0} \boldsymbol{b}_{n} + \boldsymbol{b}_{n}^{\dagger} \boldsymbol{t}_{0} \boldsymbol{b}_{n+1} \right).$$

$$(3)$$

 $a_n(b_n)$  and  $a_n^{\dagger}(b_n^{\dagger})$  are the annihilation and creation operators, respectively of the source (drain).

 $H_T$  describes the coupling of the ring with S and D, and it is also expressed in the usual TB form.

## B. Circular current density

We evaluate the spin-dependent circular current density within the ring adopting wave-guide theory, where we solve the Schrödinger equation

$$H|\psi\rangle = EI|\psi\rangle.$$
 (4)

I is the  $(2 \times 2)$  identity matrix. The wave function  $|\psi\rangle$ , representing the entire system has the form:

$$|\psi\rangle = \left[\sum_{n \le -1} A_n a_n^{\dagger} + \sum_{n \ge 1} B_n b_n^{\dagger} + \sum_{i=1} C_i c_i^{\dagger}\right] |0\rangle. \quad (5)$$

The coefficients 
$$\boldsymbol{A}_n = \begin{pmatrix} A_{n,\sigma\sigma'} \\ A_{n,\sigma\sigma'} \end{pmatrix}$$
,  $\boldsymbol{B}_n = \begin{pmatrix} B_{n,\sigma\sigma'} \\ B_{n,\sigma\sigma'} \end{pmatrix}$ , and  $\boldsymbol{C}_i = \begin{pmatrix} C_{i,\sigma\sigma'} \\ C_{i,\sigma\sigma'} \end{pmatrix}$  correspond to the amplitudes for an electron at the *n*-th site of the source, drain, and *i*-th site of the ring, respectively. From Eq. (4) we get a set of coupled equations as:

$$\begin{bmatrix}
\begin{pmatrix} E & 0 \\ 0 & E \end{pmatrix} - \begin{pmatrix} \epsilon_{0} & 0 \\ 0 & \epsilon_{0} \end{pmatrix} \end{bmatrix} \begin{pmatrix} A_{n,\sigma\sigma'} \\ A_{n,\sigma\sigma'} \end{pmatrix} = \begin{pmatrix} t_{0} & 0 \\ 0 & t_{0} \end{pmatrix} \begin{pmatrix} A_{n+1,\sigma\sigma'} \\ A_{n+1,\sigma\sigma} \end{pmatrix} + \begin{pmatrix} t_{0} & 0 \\ 0 & t_{0} \end{pmatrix} \begin{pmatrix} A_{n-1,\sigma\sigma'} \\ A_{n-1,\sigma\sigma'} \end{pmatrix}, \quad n \leq -2,$$

$$\begin{bmatrix} \begin{pmatrix} E & 0 \\ 0 & E \end{pmatrix} - \begin{pmatrix} \epsilon_{0} & 0 \\ 0 & \epsilon_{0} \end{pmatrix} \end{bmatrix} \begin{pmatrix} A_{-1,\sigma\sigma'} \\ A_{-1,\sigma\sigma'} \end{pmatrix} = \begin{pmatrix} t_{0} & 0 \\ 0 & t_{0} \end{pmatrix} \begin{pmatrix} A_{-2,\sigma\sigma'} \\ A_{-2,\sigma\sigma'} \end{pmatrix} + \begin{pmatrix} t_{S} & 0 \\ 0 & t_{S} \end{pmatrix} \begin{pmatrix} C_{N_{S},\sigma\sigma'} \\ C_{N_{S},\sigma\sigma'} \end{pmatrix},$$

$$\begin{bmatrix} \begin{pmatrix} E & 0 \\ 0 & E \end{pmatrix} - \begin{pmatrix} \epsilon_{0} & 0 \\ 0 & \epsilon_{0} \end{pmatrix} \end{bmatrix} \begin{pmatrix} B_{n,\sigma\sigma'} \\ B_{n,\sigma\sigma'} \end{pmatrix} = \begin{pmatrix} t_{0} & 0 \\ 0 & t_{0} \end{pmatrix} \begin{pmatrix} B_{n+1,\sigma\sigma'} \\ B_{n+1,\sigma\sigma} \end{pmatrix} + \begin{pmatrix} t_{0} & 0 \\ 0 & t_{0} \end{pmatrix} \begin{pmatrix} B_{n-1,\sigma\sigma'} \\ B_{n-1,\sigma\sigma'} \end{pmatrix}, \quad n \geq 2$$

$$\begin{bmatrix} \begin{pmatrix} E & 0 \\ 0 & E \end{pmatrix} - \begin{pmatrix} \epsilon_{0} & 0 \\ 0 & \epsilon_{0} \end{pmatrix} \end{bmatrix} \begin{pmatrix} B_{1,\sigma\sigma'} \\ B_{1,\sigma\sigma'} \end{pmatrix} = \begin{pmatrix} t_{0} & 0 \\ 0 & t_{0} \end{pmatrix} \begin{pmatrix} B_{2,\sigma\sigma'} \\ B_{2,\sigma\sigma'} \end{pmatrix} + \begin{pmatrix} t_{D} & 0 \\ 0 & t_{D} \end{pmatrix} \begin{pmatrix} C_{N_{D},\sigma\sigma'} \\ C_{N_{D},\sigma\sigma'} \end{pmatrix},$$

$$\begin{bmatrix} \begin{pmatrix} E & 0 \\ 0 & E \end{pmatrix} - \begin{pmatrix} \epsilon_{i} & 0 \\ 0 & \epsilon_{i} \end{pmatrix} \end{bmatrix} \begin{pmatrix} C_{i,\sigma\sigma} \\ C_{i,\sigma\sigma} \end{pmatrix} = \begin{pmatrix} t & -\imath\alpha e^{-\imath\varphi_{i,i+1}} & t \\ -\imath\alpha e^{-\imath\varphi_{i,i+1}} & t \end{pmatrix} \begin{pmatrix} C_{i+1,\sigma\sigma} \\ C_{i+1,\sigma\sigma} \end{pmatrix} + \begin{pmatrix} t_{S} & 0 \\ 0 & t_{S} \end{pmatrix} \begin{pmatrix} C_{N_{S},\sigma\sigma'} & 0 \\ 0 & t_{S} \end{pmatrix} \begin{pmatrix} C_{N_{S},\sigma\sigma'} & 0 \\ 0 & t_{S} \end{pmatrix} \delta_{i,N_{S}} + \begin{pmatrix} t_{D} & 0 \\ 0 & t_{D} \end{pmatrix} \begin{pmatrix} C_{N_{D},\sigma\sigma'} \\ C_{N_{D},\sigma\sigma'} \end{pmatrix} \delta_{i,N_{D}}, \quad 1 \leq i \leq N.$$
(6)

 $\sigma$  represents up and down spins and similarly  $\sigma'$  also.  $t_S$  and  $t_S$  are the couplings between the source and the drain to the  $N_S$ -th and  $N_D$ -th sites of the ring, respectively.

Depending upon the nature of incident electrons, now we consider two different situations.

# (i) Up spin incidence from the source lead:

In this case, we consider that an up spin electron incidents as a plane wave with unit amplitude, having the form:

$$\mathbf{A}_{n} = \begin{pmatrix} e^{ik(n+1)a} + r_{\uparrow\uparrow}e^{-ik(n+1)a} \\ r_{\uparrow\downarrow}e^{-ik(n+1)a} \end{pmatrix} \text{ and }$$

$$\mathbf{B}_{n} = \begin{pmatrix} \tau_{\uparrow\uparrow}e^{ikna} \\ \tau_{\uparrow\downarrow}e^{ikna} \end{pmatrix},$$

where a being the lattice spacing and k is the wave vector associated with the energy E.  $\tau_{\uparrow\uparrow}$   $(\tau_{\uparrow\downarrow})$  and  $r_{\uparrow\uparrow}$   $(r_{\uparrow\downarrow})$  are the transmission and reflection amplitudes of an up spin, transmitted, and reflected as up (down) spin, respectively.

Putting the expression of  $\mathbf{A}_n$  and  $\mathbf{B}_n$  in Eq. (6), we solve the wave amplitudes  $C_{i,\uparrow\sigma}$ s and the transmission amplitudes  $t_{\uparrow\sigma}$ ,  $\sigma = \uparrow, \downarrow$  for a particular energy associated with wave vector k. We finally get the spin-dependent transmission probability and the bond current density between the sites i and i+1 of the ring as:

$$T_{\uparrow\sigma} = |\tau_{\uparrow\sigma}|^2 \tag{7}$$

and

$$J_{i \to i+1 \uparrow \sigma} = \frac{\sqrt{t^2 + \alpha^2} \operatorname{Im} \left[ C_{i,\uparrow\sigma}^* C_{i+1,\uparrow\sigma} \right]}{(1/2) t_0 \sin(ka)}, \sigma \to \uparrow, \downarrow,$$
(8)

respectively.

# (ii) Down spin incidence from the source lead:

For this case, down spin incidents with unit amplitudes, where  $\mathbf{A}_n$  and  $\mathbf{B}_n$  look like:

$$\begin{split} \boldsymbol{A_n} &= \left( \begin{array}{c} r_{\downarrow\uparrow} e^{-ik(n+1)a} \\ e^{ik(n+1)a} + r_{\downarrow\downarrow} e^{-ik(n+1)a} \end{array} \right) \text{ and } \\ \boldsymbol{B_n} &= \left( \begin{array}{c} \tau_{\downarrow\uparrow} e^{ikna} \\ \tau_{\downarrow\downarrow} e^{ikna} \end{array} \right), \end{split}$$

respectively.  $\tau_{\downarrow\uparrow}$   $(\tau_{\downarrow\downarrow})$  and  $r_{\downarrow\uparrow}$   $(r_{\downarrow\downarrow})$  are the transmission and reflection amplitudes for down spin transmitted and reflected as up (down) spin, respectively.

Using the same prescription as stated for the case of up spin incidence, we calculate the transmission probabilities and bond current densities for the down spin incidence as follows

$$T_{\downarrow \sigma} = |\tau_{\downarrow \sigma}|^2 \tag{9}$$

and

$$J_{i \to i+1, \downarrow \sigma} = \frac{\sqrt{t^2 + \alpha^2} \operatorname{Im} \left[ C_{i, \downarrow \sigma}^* C_{i+1, \downarrow \sigma} \right]}{(1/2) t_0 \sin(ka)}, \sigma \to \uparrow, \downarrow,$$
(10)

respectively.

From the bond current density, we finally calculate the circular current density flowing within the ring as:

$$J_{\sigma,\sigma'} = \frac{1}{N} \sum_{i} J_{i \to i+1,\sigma\sigma'}, \quad \sigma, \sigma' \to \uparrow, \downarrow. \tag{11}$$

#### C. Circular Current

The net circular current within the ring, for a particular bias voltage V at absolute zero temperature, can be evaluated from the relation

$$I_{\sigma\sigma'}(V) = \int_{E_F - \frac{eV}{2}}^{E_F + \frac{eV}{2}} J_{\sigma\sigma'}(E) dE, \quad \sigma, \sigma' \to \uparrow, \downarrow. \quad (12)$$

 $E_F$  is the equilibrium Fermi energy. The net up and down-spin currents are defined as:

$$I_{\uparrow} = I_{\uparrow\uparrow} + I_{\downarrow\uparrow}, I_{\downarrow} = I_{\uparrow\downarrow} + I_{\downarrow\downarrow},$$
 (13)

respectively<sup>19</sup>. Using  $I_{\uparrow}$  and  $I_{\downarrow}$ , we define the net charge and spin currents as

$$I_C = I_{\uparrow} + I_{\downarrow},$$
  

$$I_S = I_{\uparrow} - I_{\downarrow},$$
(14)

respectively<sup>19</sup>.

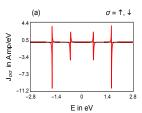
#### III. RESULTS AND DISCUSSIONS

There are a few parameters that are kept constant throughout the paper. The onsite potentials are chosen to be zero, i.e.,  $\epsilon_0 = \epsilon_n = 0 \ \forall \ n$ . The nearest-neighbor hopping integrals are taken as:  $t_0 = 2\,\mathrm{eV},\ t = 1\,\mathrm{eV},$  and  $t_S = t_D = 0.5\,\mathrm{eV}$ . The source is always connected to the first site of the ring, which is  $N_S = 1$ . We consider the lattice spacing a as  $1\mathring{A}$ . Current moving at the counter-clockwise direction in any segment of the ring is considered to be positive.

# A. Without Spin Orbit Interaction

First, we try to understand the basic features of the current density without any spin-orbit interaction. When the ring is symmetrically connected to the source and drain, the net circular current becomes zero. Therefore we concentrate on asymmetric ring-to-lead configuration (Fig. 2). The ring has 10 atomic sites. The drain is connected at the 7-th site of the ring. In Fig. 2(a) we plot the  $J_{\sigma\sigma}$  ( $\sigma=\uparrow$  or  $\downarrow$ ) with energy E. Both the  $J_{\uparrow\uparrow}$  and  $J_{\downarrow\downarrow}$  are the same, as no spin scattering interaction is present in the system. For the same reason, the spin current densities corresponding to the spin flipping process  $(J_{\uparrow\downarrow})$  and  $J_{\downarrow\uparrow}$ ) are also zero here. The energies associated

with the picks and the dips in the spectra correspond to the energy eigenvalues of the ring. For our present choice of parameter values, the eigenvalues of the ring Hamiltonian (written in Eq. (2)) without any spin-orbit interaction ( $\alpha=0$ ) are:  $-2, -2, -1.62, -1.62, -1.62, -1.62, -0.62, -0.62, -0.62, -0.62, 0.62, 0.62, 0.62, 0.62, 1.62, 1.62, 1.62, 1.62, 2.0, 2.0 eV. Along with the two fold spin degeneracy of each energy level, the system has another doubly degenerate energy levels due to the periodic boundary condition <math>N+1\equiv 1$  which leads to the energy dispersion as  $E=2t\mathrm{Cos}(ka)$  where  $k=2\pi m/Na$ . The



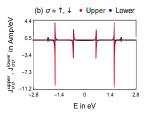


FIG. 2: (Color online). (a) Current density  $J_{\sigma\sigma}$  as a function of energy E. (b) Current densities flowing at the upper and lower arms of the ring.

integer m runs between  $N/2 \le m < N/2$ . Therefore for k and -k, the system has the same energy except at m=0for odd N and m = -N/2, 0 for even N. For example, in our present setup, N = 10. Therefore the degeneracies appear when  $m = \pm 4, \pm 3, \pm 2,$  and  $\pm 1$ . Whereas the energy levels corresponding to m=-5, that is  $E=-2\,\mathrm{eV}$ and m=0 with  $E=-2\,\mathrm{eV}$ , remain non-degenerate. The doubly degenerate orbitals are characterized by their orbital angular momentum, representing Bloch waves traveling clockwise or counter-clockwise along the ring. The circular current appears within the ring when this degeneracy is lifted due to the ring-to-leads coupling. The symmetric ring-to-lead connection does not split the degeneracies hence a net circular current (specifically charge circular current) does not appear. Whereas, for an asymmetric connection, there is a net current within the ring.

The current densities flowing through the upper and lower arms  $(J_{\sigma\sigma}^{upper}$  and  $J_{\sigma\sigma}^{lower}$ , respectively) are plotted in Fig. 2(b). As we can see,  $J_{\sigma\sigma}^{upper}$  is opposite in sign to the  $J_{\sigma\sigma}^{lower}$  at non-degenerate energy levels. But they flow in the same direction at degenerate energy levels. The slight splitting at these degenerate levels are caused by the coupling of the ring with the electrodes. The current density in terms of  $J_{\sigma}^{upper}$  and  $J_{\sigma}^{lower}$  can be written as

$$J_{\sigma} = f^{\text{upper}} J_{\sigma}^{\text{upper}} + f^{\text{lower}} J_{\sigma}^{\text{lower}}.$$
 (15)

 $f^{\rm upper}=(N_D-1)/N$  and  $f^{\rm lower}=(N-N_D+1)/N$  are the weight factors for the upper and lower arms, respectively. As across  $E=\pm 2\,{\rm eV}$ , the current flows in the two arms of the ring in opposite directions, with almost equal magnitude, vanishingly small current densities are obtained. Whereas at the degenerate energies (neglecting spin degeneracy), the contributions from both of the arms are additive, hence a net circular current density is obtained.

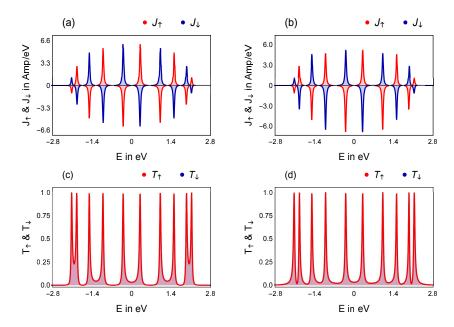


FIG. 3: (Color online). (a) - (b) Up and down spin current densities and (c) - (d) up and down spin transmission probabilities with energy for  $\alpha = 0.4 \,\text{eV}$ . The left column ((a) and (c)) represent symmetric ring-to-lead connection whereas right column i.e. (b) and (d) are simulated for most asymmetric configuration (i.e.,  $N_D = 10$ ). The other parameters are same as Fig. 2.

# B. With Spin Orbit Interaction

The Rashba spin-orbit interaction causes momentum-dependent spin splitting of electronic bands. But with non-zero SOI, the quantum ring still has at least one more eigenstate with the same energy according to the Kramers degeneracy theorem as our spin-half system preserves time-reversal symmetry. Circular current (as well as non-zero transmission probability) appears for corresponding energy eigenvalues similar to the previous situation (for Rashba spin-orbit interaction strength  $\alpha = 0.4 \,\mathrm{eV}$  and with our present choices of parameters, these energies are: -2.12, -2.12, -1.94, -1.94, -1.5, -1.5, -1.01, -1.01, -0.3, -0.3, 0.3,0.3, 1.01, 1.01, 1.5, 1.5, 1.94, 1.94, 2.12, and 2.12 eV.) The effect of spin-orbit interaction on current density as well as on the transmission spectra is studied in Fig. 3 for symmetric and asymmetric connections.

As for the two terminal SOI device, magnetic field (to break the time reversal symmetry) is a key ingredient to

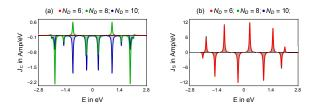


FIG. 4: (Color online). Charge  $(J_C)$  and spin  $(J_S)$  current densites with energy E for N=10 and  $\alpha=0.4\,\mathrm{eV}$ . In each case we calculate the current for three different ring-to-lead configurations. The red curve corresponds to  $N_D=6$ , whereas for green and blue curves we choose  $N_D=8$  and 10, respectively.

produce an net spin-polarized current at outgoing termi-

nal, in the transmission probability we do not observe any spin-separation for symmetric (Fig. 3(c)) as well as asymmetric (Fig. 3(d)) cases. But within the conductor a net spin current appears for both the cases (Fig. 3(a) -(b)). In fact for the symmetric case (Fig. 3(a)), we have

$$J_{\uparrow}(\pm E) = -J_{\downarrow}(\pm E). \tag{16}$$

Therefore, in this situation, throughout the energy window, the net charge current density

$$J_C(E) = J_{\uparrow}(E) - J_{\downarrow}(E) = 0.$$
 (17)

But net spin current density,

$$J_S(E) = J_{\uparrow}(E) - J_{\downarrow}(E)$$
  
=  $2J_{\uparrow}(E) = -2J_{\downarrow}(E)$ . (18)

Hence a pure spin current appears (charge current is zero). Apart from equality relations stated in Eq. (16), for symmetric connection, we also have

$$J_{\uparrow}(E) = -J_{\uparrow}(-E),$$
  

$$J_{\downarrow}(E) = -J_{\downarrow}(-E).$$
(19)

Equation (19) implies,

$$J_S(E) = J_{\uparrow}(E) - J_{\downarrow}(E)$$

$$= J_{\downarrow}(-E) - J_{\uparrow}(-E)$$

$$= -J_S(-E). \tag{20}$$

As the net spin current  $I_S$  at a voltage V is given by the area under the  $J_S - E$  (Eq. (12)), therefore net  $I_S$  is zero under the condition  $E_F = 0$ . Therefore to get pure spin current, we need to set Fermi energy  $E_F$  other than zero.

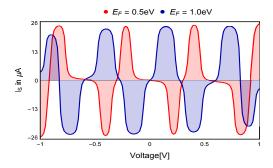


FIG. 5: (Color online). Superposition of net spin currents  $I_{SS}$  with bias voltage V for a symmetric (red curve) and most asymmetric (blue curve) connections. The results are computed for a 40 site ring for two different Fermi-energies ( $E_F$ ). The strength of spin-orbit interaction is  $0.2 \,\mathrm{eV}$ .

For the asymmetric connection (Fig. 3(b)), when there is a splitting in the degeneracy, we have a net charge as well as spin circular currents. In this condition, the up and down components of the circular current density are opposite to each other but they are not equal, that is:

$$J_{\uparrow}(\pm E) \neq -J_{\downarrow}(\pm E).$$
 (21)

But similar to the symmetric connection condition, for asymmetric connection we still have,

$$J_{\uparrow}(E) = J_{\downarrow}(-E),$$
  

$$J_{\downarrow}(E) = J_{\uparrow}(-E).$$
 (22)

Therefore, under asymmetric connection,

$$J_C(E) = J_{\uparrow}(E) + J_{\downarrow}(E)$$

$$= J_{\downarrow}(-E) + J_{\uparrow}(-E)$$

$$= J_C(-E). \tag{23}$$

But for the net spin current we have,

$$J_{S}(E) = J_{\uparrow}(E) - J_{\downarrow}(E)$$

$$= J_{\downarrow}(-E) - J_{\uparrow}(-E)$$

$$= -J_{S}(-E). \tag{24}$$

Therefore the spin  $I_S$  current vanishes for  $E_F=0$  similar to the symmetric connection situation. But as the charge current density is symmetric around E=0, we can get a pure charge current setting the Fermi energy at 0.

The total charge current density  $J_C$  is plotted in Fig. 4(a) for three different ring-to-leads configurations. In Fig. 4(b), we calculate the spin current density for the same, though as they are almost similar. There a are few basic differences between  $J_C$  and  $J_S$  that we can see in Fig. 4. (i) In each case a total of 10 peaks and dips are visible there but for spin current density the subsequent energy levels carry currents in opposite directions, whereas no such sequence is seen for charge current density. (ii)  $J_C$  is symmetric around E=0, whereas  $J_S$  is anti-symmetric. In other words  $J_C(E)=J_C(-E)$  and  $J_S(E)=-J_S(-E)$ , as we have already found in Eq. (20), Eq. (23) and 24. (iii) The charge current density is very much sensitive to the ring-lead connection positions, but  $J_S$  is quite independent of that.

# C. Spin current

Now we calculate the total pure spin current. In Fig. 5

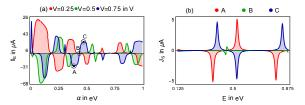


FIG. 6: (Color online).(a) Variation of pure spin current  $I_S$  with Rashba spin-orbit interaction  $\alpha$  in a symmetric 30-size junction at three different voltages. (b) Spin current densities at three different values of  $\alpha$ , those are marked by encircled dots in (a).

we plot the pure spin current  $I_S$  with voltage V setting Fermi energy at  $E_F = 0.5 \,\text{eV}$  (red) and  $E_F = 1 \,\text{eV}$  (blue). The ring has 40 atomic sites and is symmetrically connected to the drain at  $N_D = 21$ .  $I_S$  shows oscillation with voltage V, for both the choices of the Fermi energies. For a very small voltages around zero, the current is vanishingly small as no resonant energy level appears within the window. Current becomes finite when anyone of such energy levels lies within the voltage window. As we further increase the voltage, more and more resonant energy levels appear within the window. Depending on their contributions to the net current, the circular current becomes positive or negative, or zero. As the spin circular current density remains almost unchanged with the connection position of the drains, the current-voltage spectra are almost the same, for the other ring-to-lead configurations with fixed N.

In order to see the dependence of pure spin current on spin-orbit interaction we present its variations as a function of  $\alpha$  for some typical values of bias voltage V in Fig. 6(a).  $I_S$  has an oscillatory behavior with  $\alpha$  and its sign alternately changes from positive to negative for a wide window of  $\alpha$ . Therefore we can control the  $I_S$ by spin-orbit interaction without disturbing any physical parameters of the system and can be utilized in designing effective spin-based quantum devices. To explain this large variation of the spin current with SOI, we choose three distinct points A, B, and C from  $I_S - \alpha$  curve of Fig. 6(a), represented by encircled dots, and present the current densities for the corresponding values of  $\alpha$ in Fig.6(b). The results are shown for a specific energy window (0.125  $\leq E \leq$  0.875) associated with the voltage  $V = 0.75 \,\mathrm{V}$  and Fermi-energy  $E_F = 0.5 \,\mathrm{eV}$ . For the  $\alpha$ value associated with point A, two current density peaks appear at negative energy while there is only one positive energy peak (shown by the red color curve in Fig.6(b)), which results in a net negative circular current. The scenario gets reversed at the  $\alpha$  value associated with point C (shown by the blue color in Fig.6(b)). Therefore a net positive current flows in the ring. At the  $\alpha$  value associated with point B, the current densities obtained for both positive and negative energies are closely equal (shown by the green color curve in Fig.6(b)). Therefore vanishing spin current appears in this case.

#### IV. CONCLUSION

In summary, we have discussed the effects of Rashba spin-orbit interaction on the circular current, which appears within a conductor having loop geometry. We have discussed the origin of the circular currents from the degeneracy point of view. We have found that, in a symmetric junction, the charge circular current is always zero, but in this case, we have got non-zero pure spin circular current (i.e., minimization of the Joule heating) setting the Fermi-energy at any value other than zero. The system has double degeneracy which can be characterized by its orbital angular momentum. On the other hand, in an asymmetric junction, we have got a pure charge current, setting Fermi-energy at zero. Due to ring-to-electrodes coupling, the degeneracy is removed here.

Finally, we have shown a way to regulate the pure spin current by changing the strength of spin-orbit interaction. Our results will serve to design the new generation spintronic devices where only spin will carry the information.

#### V. ACKNOWLEDGEMENTS

The author acknowledges the financial support by the Postdoctoral Fellowship of Indian Institute of Science Education and Research, Pune, India and the Japan Society for the Promotion of Science Postdoctoral Fellowship for Research in Japan (JSPS, ID No. P21022). The Author is thankful to Bijay Kumar Agarwalla and Santanu K. Maiti for numerous useful discussions.

- <sup>1</sup> M. Büttiker, Y. Imry, R. Landauer, Phys. Lett. A **96**, 365 (1983).
- <sup>2</sup> L.P. Lévy, G. Dolan, J. Dunsmuir, H. Bouchiat, Phys. Rev. Lett. **64**, 2074 (1990).
- <sup>3</sup> V. Ambegaokar, U. Eckern, Phys. Rev. Lett. **65**, 381 (1990).
- <sup>4</sup> V. Chandrasekhar, R.A. Webb, M.J. Brady, M.B. Ketchen, W.J. Gallagher, A. Kleinsasser, Phys. Rev. Lett. **67**, 3578 (1991).
- <sup>5</sup> E.M.Q. Jariwala, P. Mohanty, M.B. Ketchen, R.A. Webb, Phys. Rev. Lett. **86**, 1594 (2001).
- <sup>6</sup> N.O. Birge, Science **326**, 244 (2009).
- <sup>7</sup> H. Bluhm, N.C. Koshnick, J.A. Bert, M.E. Huber, K.A. Moler, Phys. Rev. Lett. **102**, 136802 (2009).
- Yu. V. Pershin and C. Piermarocchi, Phys. Rev. B 72, 245331 (2005).
- <sup>9</sup> O. Entin-Wohlman, Y. Imry, A. Aharony, Phys. ReV. Lett. 91 046802, (2003).
- <sup>10</sup> A. Matos-Abiague and J. Berakdar, Phys. ReV. Lett. **94**, 166801 (2005).
- <sup>11</sup> S. S. Gylfadottir, M. Nita, V. Gudmundsson, A. Manolescu, Phys. E 27, 278 (2005).
- <sup>12</sup> I. Barth, J. Manz, and Y. Shigeta, and K. J. Yagi, Am. Chem. Soc. **128**, 7043 (2006).
- <sup>13</sup> G. F. Quinteiro and J. Berakdar, Opt. Express **17**, 20465 (2009).
- <sup>14</sup> G. Stefanucci, E. Perfetto, S. Bellucci, and M. Cini, Phys. Rev. B **79**, 073406 (2009).
- <sup>15</sup> D. Rai, O. Hod, and A. Nitzan, J. Phys. Chem. C **114**, 20583 (2010).
- <sup>16</sup> D. Rai, O. Hod, and A. Nitzan, Phys. Rev. B 85, 155440 (2012).
- <sup>17</sup> S. K. Maiti, J. Appl. Phys. **117**, 024306 (2015).
- <sup>18</sup> M. Patra and S. K. Maiti, Sci. Rep. **7**, 43343 (2017).
- <sup>19</sup> M. Patra and S. K. Maiti, Phys. Rev. B **100**, 165408 (2009).
- <sup>20</sup> S. Nakanishi and M. Tsukada, Phys. Rev. Lett 87, 126801

- (2001).
- <sup>21</sup> N. Tsuji, S. Takajo, and H. Aoki, Phys. Rev. B **75**, 153406 (2007).
- <sup>22</sup> G. Burkard, D. Loss, and D. P. DiVincenzo, Phys. Rev. B 59, 2070 (1999).
- <sup>23</sup> R. Vrijen, E. Yablonovitch, K.Wang, H.W. Jiang, A. Balandin, V. Roychowdhury, T. Mor, and D. DiVincenzo, Phys. Rev. A 62, 012306 (2000).
- <sup>24</sup> D. Rai and M. Galperin, Phys. Rev. B **86**, 045420 (2012).
- <sup>25</sup> M. Patra and S. K. Maiti, Org. Electron. **62**, 454 (2018).
- <sup>26</sup> M. Patra, A. Shukla, and S. K. Maiti, J. Phys. D: Appl. Phys. **54**, 095001 (2021).
- <sup>27</sup> Y. Feng, et al., Nat Commun. **10**, 4765 (2019).
- <sup>28</sup> Y.A. Bychkov, E.I. Rashba, J. Exp. Theor. Phys. Lett. **39**, 78 (1984)
- <sup>29</sup> A. Manchon, H. Koo, J. Nitta, S. M. Frolov, and R. A. Duine, Nature Mater **14**, 871 (2015).
- <sup>30</sup> L. Meier, G. Salis, I. Shorubalko, E. Gini, S. Schön, K. Ensslin, Nat. Phys. 3, 650 (2007).
- <sup>31</sup> P. Wadley, Nature Mater **17**, 566 (2018).
- <sup>32</sup> S. Y. Huang, D. Qu, T. C. Chuang, C. C. Chiang, W. Lin, and C. L. Chien, Appl. Phys. Lett. **117**, 190501 (2020).
- <sup>33</sup> S. Y. Huang, D. Qu, T. C. Chuang, C. C. Chiang, W. Lin, and C. L. Chien, Appl. Phys. Lett. **117**, 190501 (2020).
- <sup>34</sup> J. E. Hirsch, Phys. Rev. Lett. **83**, 1834 (1999).
- <sup>35</sup> Y. Tserkovnyak, A. Brataas, and G. E. W. Bauer, Phys. Rev. Lett. 88, 117601 (2002).
- <sup>36</sup> C.-M. Ryu, S. Y. Cho, M. Shin, K. W. Park, S. Lee, and E.-H. Lee, Int. J. Mod. Phys. B **10**, 701 (1996).
- <sup>37</sup> Y. Shi and H. Chen, Phys. Rev. B **60**, 10949 (1999).
- <sup>38</sup> Y.-J. Xiong and X.-T. Liang, Phys. Lett. A **330**, 307 (2004).
- <sup>39</sup> J. C. Slater and G. F. Koster, Phys. Rev. **94**, 1498 (1954).
- <sup>40</sup> C. Delerue and M. Lannoo, Nanostructures: Theory and Modelling (Springer, New York, 2004).